Available online at www.sciencedirect.com
ScienceDirect
Journal of Nuclear Materials 363–365 (2007) 1066–1070
journal of nuclear materials
www.elsevier.com/locate/jnucmat

Particle flux and radial profiles in the SOL of DIII-D during ELMing H-mode

A.W. Leonard [a,*], J.A. Boedo [b], M. Groth [c], B.L. Lipschultz [d], G.D. Porter [c], D.L. Rudakov [b], D.G. Whyte [e]

[a] General Atomics, P.O. Box 85608, San Diego, CA 92186-5608, USA
[b] University of California-San Diego, La Jolla, CA, USA
[c] Lawrence Livermore National Laboratory, Livermore, CA, USA
[d] Massachusetts Institute of Technology, Cambridge, MA, USA
[e] University of Wisconsin, Madison, WI, USA

Abstract

The radial particle flux in the scrape-off-layer (SOL) during ELMing H-mode is examined in DIII-D as a function of density. The global radial particle flux in the outboard far SOL is determined by a window frame technique. Between ELMs, the outboard far SOL particle flux increases strongly with density and remains similar to the particle flux across the separatrix as estimated by the pedestal density and temperature gradients. At low density the steep density gradient of the pedestal extends up to 2 cm outside the separatrix, while at high density the density gradient flattens just outside the separatrix. During ELMs the far SOL particle flux becomes localized to the outboard midplane and the assumptions for the window frame analysis break down. Implications for scaling of outboard main chamber wall particle flux and pedestal fueling are explored.

PACS: 52.55.Fa; 52.25.Fi

Keywords: Particle flux; Cross-field transport; Recycling; DIII-D; ELMs

1. Introduction

Particle flux to plasma facing components is largely responsible for the generation of plasma impurities, and its distribution can affect plasma flow and fueling of the pedestal. Several studies examined the contributions of scrape-off-layer (SOL) radial particle transport in the outboard main chamber to the overall surface particle flux in DIII-D [1–5]. Radial transport in the far SOL can be large and convective in nature, leading to significant particle flux to the main chamber, particularly at high density [3,4]. While many of these studies examined L-mode, some data in H-mode with edge localized modes (ELMs) indicate that the wall flux at the outboard midplane can be dominated by the particle flux

* Corresponding author. Fax: +1 858 455 4156.
E-mail address: leonard@fusion.gat.com (A.W. Leonard).

0022-3115/$ - see front matter
doi:10.1016/j.jnucmat.2007.01.248

during ELMs, particularly at low density [5]. Detailed comparison of modeling and data of the 2D recycling profile in DIII-D at low density ($n_e/n_{GW} \sim 0.3$) indicates, however, that the pedestal can still be largely refueled from the divertor region [6].

This study examines the consistency of the previous measurements and their implications for global particle fluxes, and their recirculation, in the context of ELMing H-mode as a function of density. The particle flux across the separatrix is compared to fluxes to the outboard main chamber and the divertor target, with the fluxes between ELMs and during ELMs treated separately.

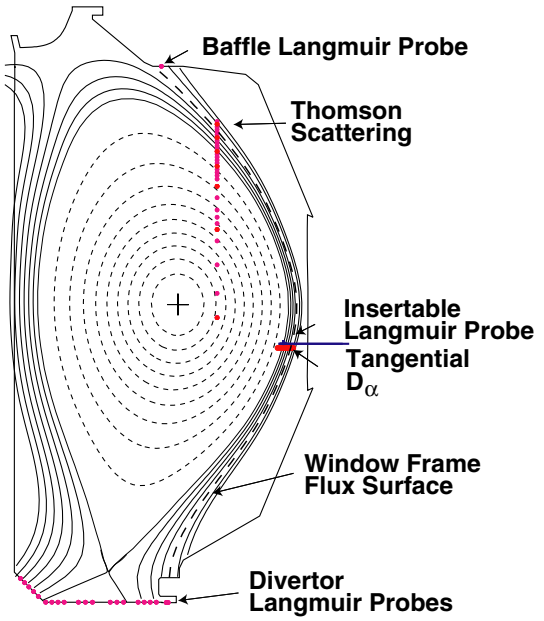

Fig. 1. The diagnostics and magnetic configuration used in this study. Shown are the edge Thomson scattering, a fixed upper baffle Langmuir probe, the midplane insertable Langmuir probe, the edge tangential D_α array and the lower divertor Langmuir probes. Also shown is the magnetic surface used for the window frame particle flux analysis.

2. Experimental setup

This study was carried out in a lower single-null configuration, Fig. 1, with a plasma current of 1.0 MA, toroidal field of 1.7 T for q_{95} of ~4.3 and constant neutral beam injected power of 4.8 MW. The density was scanned discharge to discharge with divertor pumping for low density and external gas puffing for higher density. The density scan achieved a pedestal density variation from 2.5 to 6.4×10^{19} m^{-3}, or $n_{e,ped}/n_{Greenwald(GW)} \sim 25$–65%. The Type I ELMs maintained a frequency of 80 Hz over this density range, though with larger fluctuations in the midplane D_α signals between ELMs at higher density.

The diagnostics for this study are also shown in Fig. 1. Thomson data for the pedestal and near SOL profiles is sorted with respect to ELM phase to obtain separate profiles between and during ELMs. Typical electron density and temperature profiles between ELMs are shown in Fig. 2. The outboard midplane far SOL plasma is measured with an insertable Langmuir probe, Fig. 1. The probe plunges twice each shot to the same flux surface as the corner of the upper baffle, a toroidally symmetric surface. Typical profiles from the probe are shown in Fig. 2. The insertable probe measurements are compared with a fixed Langmuir probe on the upper baffle and probes on the lower divertor target.

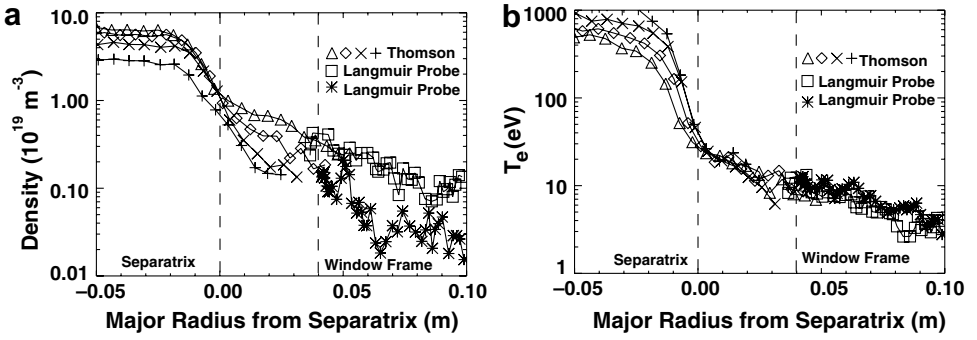

Fig. 2. The pedestal and edge (a) density and (b) electron temperature between ELMs from Thomson scattering and the midplane Langmuir probe. Four representative profiles from the density scan are shown for the Thomson data. A high and low density case are shown for the midplane probe.

3. Separatrix particle flux

In a previous DIII-D study [7] examining the density rise just after the H-mode transition, the separatrix flux was estimated by a flux-surfaced averaged particle diffusivity, $D_\perp$, in the pedestal. The diffusivity was roughly 25% ± 10% of the effective thermal diffusivity, χ_{eff}, over a range of conditions including plasma current, density and input power. Using a tanh function fit to the Thomson profiles and setting the separatrix location at the foot of the temperature fit, χ_{eff} is determined from the T_e gradient at that location and the radial energy flux, assumed to be 70% of the injected power to account for radiation and ELM losses. An average ELM energy flux of 20% is typical for DIII-D and other tokamaks [8], and the variation of radiation plus ELM loss is not expected to be large over the density scan. The global separatrix particle flux is calculated from the density gradient assuming $D_\perp = 25\%$ of χ_{eff}. The resultant separatrix particle flux between ELMs from this analysis, shown in Fig. 3, is approximately $3\times10^{21}\ \text{s}^{-1}$ of deuterium ions at low density rising to $10\times10^{21}\ \text{s}^{-1}$ at the higher densities. The increase in particle current at high density is primarily due to an increased χ_{eff} and implied increased $D_\perp$. The uncertainty and scatter in the measurement is roughly 30%. The particle flux across the separatrix during ELMs is also significant and can be calculated by comparing the density profiles just before and after an ELM. A time-dependent density profile is constructed by sorting the Thomson density profiles with respect to the ELM phase [9]. The reconstructed profiles are integrated just before and after the ELM to determine the particle loss at an average ELM. The average particle loss multiplied by the ELM frequency represents the time-averaged particle flux during ELMs. This analysis for the density scan, Fig. 3, indicates the ELM flux is similar to the flux between ELMs at low density, 3×10^{21}, but rises only slightly at higher density, consistent with the constant ELM frequency.

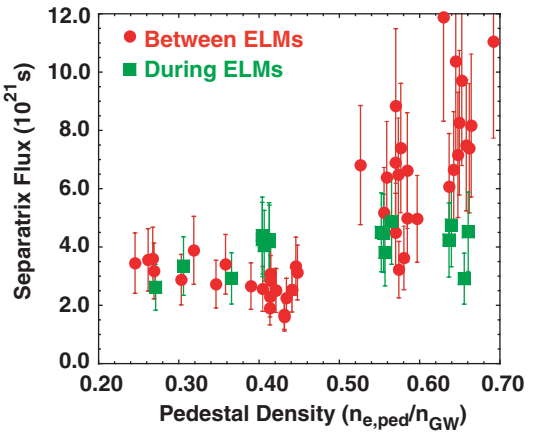

Fig. 3. Time-averaged particle flux across the separatrix between ELMs and during ELMs.

4. Far SOL particle flux

A 'window frame' analysis is used to estimate the global radial particle flux to the outboard main chamber, represented by the magnetic flux surface marked with the dashed line in Fig. 1, 4 cm from the outboard midplane separatrix [1]. An important feature of this surface is that both ends of the field lines terminate on a toroidally symmetric surface. This analysis assumes parallel plasma flow to the surface with negligible recycling in the low density far SOL plasma. Under these conditions, the particle flux through the window frame is given by Ref. [1]

$$\Gamma_i = 2\pi n_e c_s \lambda \frac{B_p}{B_T}\left[(\langle R\rangle\xi)_1 + (\langle R\rangle\xi)_2\right], \qquad (1)$$

where n_e, c_s, λ, are density and sound speed and their convoluted e-folding scale length at the midplane probe, and B_p and B_T are the midplane window frame values of toroidal and poloidal magnetic field respectively. Also R is the average major radius of the upper and lower halves of the window frame flux surface and ξ is the ratio of saturation current between the termination surfaces and the midplane, $\xi \sim 0.5$. More details and assumptions of this analysis can be found in Ref. [1].

For the midplane window frame plasma conditions, the probe profiles of electron density and temperature, Fig. 2, and ion saturation current (I_{sat}) are fit to an exponential function from the window frame radius outward to the baffle limiters. The probe and Thomson data, mapped to the midplane in Fig. 2, are generally in agreement in regions of overlap. Across the pedestal density scan of $2.5–6.4\times10^{19}\ \text{m}^{-3}$ the midplane density at the window frame radius, 4 cm outside the separatrix at the outboard midplane, increases from 1.0 to $3.5\times10^{18}\ \text{m}^{-3}$ while the electron temperature remains constant at 15 eV. The density and I_{sat} scale lengths increase from 1 to 4 cm across the density

scan while temperature scale length remains constant at ~5 cm.

The between ELM outboard window frame particle flux, Fig. 4, is calculated from the midplane measurements using the I_{sat} measurements from the probe directly for the factors n_e, c_s and λ, and are shown in Fig. 4. The separatrix fluxes between ELMs are also shown for reference. Within the measurement uncertainty, ~30%, the outboard window frame flux between ELMs is roughly equal to the total separatrix flux between ELMs. To test the window frame analysis assumptions, the flux implied by measurements of the fixed Langmuir probe in the upper baffle, Fig. 1, are also plotted in Fig. 4. The baffle radial flux is calculated from the baffle probe saturation current and an assumed falloff length consistent with the midplane measurements. At low density, the baffle probe saturation current is near the measurement resolution and could result in a lower baffle flux than the midplane measurements. At high density, the baffle probe saturation current is higher than the midplane probe and may indicate the window frame analysis is breaking down due to local recycling.

While the outboard main chamber flux between ELMs is a factor 2–3 smaller than the L-mode flux of previous studies at the same line averaged density [1,2], due to the pedestal transport barrier, the flux increases with density in both L-mode and H-mode in a similar manner. Also consistent with the previous L-mode results, an outward radial convective velocity of ~100 m/s could account for the outboard window frame flux. This study finds the density scale length outboard of the window frame surface in H-mode to increase with density. Previous L-mode studies found either a constant scale length [1] or an increasing scale length [5]. This analysis can potentially be applied to the outboard main chamber particle flux during ELMs. Averaging the midplane probe data over the first quarter of the ELM cycle produces reasonable agreement in the region of overlap with averaged Thomson data. At the midplane, the density increases much more than the electron temperature at an ELM. This is consistent with previous DIII-D ELM measurements where the ELM T_e perturbation decays much more quickly in the SOL than the ELM n_e perturbation [10]. While the window frame T_e scale length does not change significantly at an ELM, the n_e scale length rises to approximately that of T_e.

For the outboard main chamber ELM flux, the assumptions of the window frame analysis need to be tested. In Fig. 5 the baffle probe ion saturation current density is compared to the midplane probe current density on the same flux surface. Though there is much scatter in the data, the midplane saturation current density is clearly much greater than the baffle saturation current density and indicates that the window frame assumptions are not valid. This indicates the ELM flux is highly localized to the midplane. A localized midplane flux could result from strong asymmetries of the ELM perturbation or a radial velocity faster than the parallel equilibration time. Though the global outboard main chamber flux cannot be determined, the relative

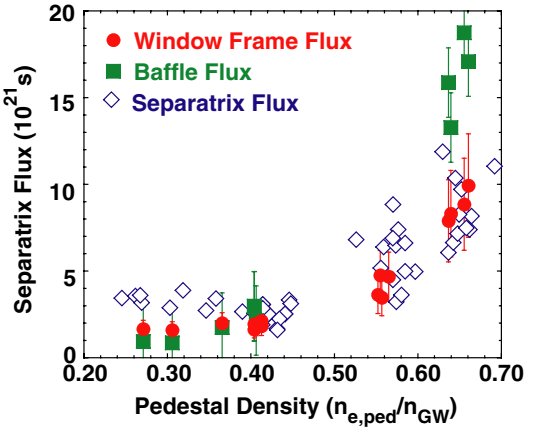

Fig. 4. The radial particle flux between ELMs through the outboard window frame as measured by the midplane probe. Also shown are the radial fluxes implied by the upper baffle Langmuir probe assuming scale lengths measured at the midplane. Also shown for reference are the fluxes across the separatrix between ELMs from Fig. 3.

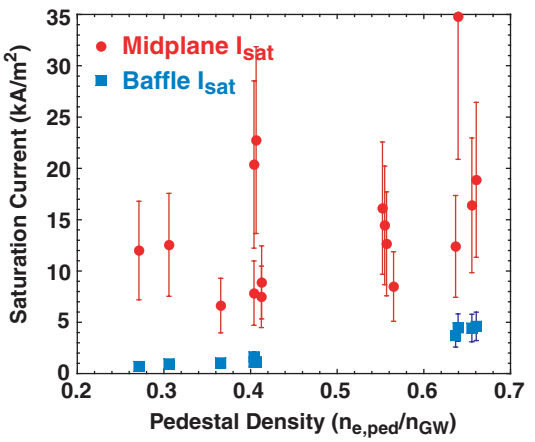

Fig. 5. The time-averaged saturation current (A/m^2) due to ELMs from the midplane Langmuir probe and the upper baffle Langmuir probe.

contribution of ELMs to the midplane flux can be estimated by comparing the time-averaged probe saturation current during ELMs to between ELMs. Using this analysis, the ELMs represent ~80% of the total midplane flux at low density, decreasing to ~60% at the higher densities. This is consistent with previous measurements where the outboard midplane flux was dominated by ELMs at low density, but became comparable to the between ELM flux at higher densities [5].

5. Summary and discussion

The outboard main chamber particle flux between ELMs was characterized and strongly increased with pedestal density, Fig. 4. The measured particle flux is consistent with convective dominated transport at ~100 m/s, a similar velocity to previously measured L-mode transport [1]. The density profiles near the separatrix exhibit qualitative changes with increasing pedestal density. Outside the separatrix at low density, the density scale length remains small up to 2 cm outside the separatrix before increasing in the far SOL. At high density, the scale length increases significantly just outside the separatrix and remains constant throughout the SOL to the outboard window frame to the midplane wall. The short scale length outside the separatrix at low density is an indication that the transport barrier can extend beyond the separatrix. The spatial extent and transport characteristics of this good confinement region must be understood to improve projections towards a large tokamak such as ITER.

The outboard main chamber particle flux during ELMs is also significant. At the midplane, particle flux is dominated by ELMs particularly at low density as was observed in a previous study [5]. The analysis of Fig. 5 indicates that the ELM flux is poloidally localized to the outboard midplane with a factor of 5 or more greater flux than to the outboard upper baffle. Further details of the ELM particle wall deposition will require more localized measurements around the periphery of the outboard main chamber.

To assess the role of outboard main chamber particle flux versus divertor flux in fueling the pedestal, particle continuity is typically assumed. This implies each particle recycles off a surface before reionization in the divertor, SOL, or core plasma setting up conserved particle loops. The contribution from ELMs can be separated from the flux between ELMs because of the short ELM time scale. The decay of the midplane D_α signal, ~1 ms, is much faster than the ELM period, ~15 ms. While the total outboard main chamber particle flux between ELMs is approximately equal to the total separatrix ion flux, within the uncertainty of approximately a factor of two, the total divertor flux, from fixed divertor Langmuir probe measurements, is roughly 10 times this value, in line with previous L-mode observations [1]. However, a smaller fraction of divertor neutrals would be expected to travel to the core plasma before ionization because of the higher divertor density. A detailed study of neutral transport, such as using a Monte Carlo neutral code with a reconstructed plasma background, is needed to assess the fueling contributions of recycling from surfaces including the divertor and main chamber. This study indicates characterizing the recycling flux from the various surfaces for modeling constraints appears feasible.

Acknowledgment

This work was supported by US Department of Energy under DE-FC02-04ER54698, DE-FC02-04ER54758, W-7405-ENG-48, DE-FC02-04ER54762, and DE-FG03-01ER54615.

References

[1] D.G. Whyte, B.L. Lipschultz, P.C. Stangeby, et al., Plasma Phys. Control. Fus. 47 (2005) 1579.
[2] B. Lipschultz, D. Whyte, B. LaBombard, Plasma Phys. Control. Fus. 47 (2005) 1559.
[3] J.A. Boedo, D.L. Rudakov, R.A. Moyer, et al., Phys. Plasmas 10 (2003) 1670.
[4] J.A. Boedo, D.L. Rudakov, R.J. Colchin, et al., J. Nucl. Mater. 313–316 (2003) 813.
[5] D.L. Rudakov, J.A. Boedo, R.A. Moyer, et al., Nucl Fusion 45 (2005) 1589.
[6] M. Groth, L.W. Owen, G.D. Porter, et al., J. Nucl. Mater. 337–339 (2005) 425.
[7] G.D. Porter, Phys. Plasmas 5 (1998) 4311.
[8] A. Herrmann, T. Eich, S. Jachmich, et al., J. Nucl. Mater. 313–316 (2003) 759.
[9] A.W. Leonard, T.H. Osborne, M.E. Fenstermacher, et al., Phys. Plasmas 10 (2003) 1765.
[10] J.A. Boedo, D.L. Rudakov, E. Hollmann, et al., Phys. Plasmas 12 (2005) 072516.